# e-MERLIN resolves Betelgeuse at λ 5 cm: hotspots at 5 $R_\star$

A. M. S. Richards,[1]⋆ R. J. Davis,[1] L. Decin,[2] S. Etoka,[1,3] G. M. Harper,[4] J. J. Lim,[5,6]
S. T. Garrington,[1] M. D. Gray,[1] I. McDonald,[1] E. O'Gorman[4] and M. Wittkowski[7]

[1]*JBCA, Department Physics and Astronomy, University of Manchester, Manchester M13 9PL, UK*
[2]*Instituut voor Sterrenkunde, Katholieke Universiteit Leuven, B-3001 Leuven, Belgium*
[3]*Hamburger Sternwarte, Gojenbergsweg 112, D-21029 Hamburg, Germany*
[4]*School of Physics, Trinity College, Dublin 2, Ireland*
[5]*Department of Physics, University of Hong Kong, Pokfulam Road, Hong Kong*
[6]*Institute of Astronomy and Astrophysics, Academia Sinica, Taipei 10617, Taiwan*
[7]*ESO, D-85748 Garching bei München, Germany*

## ABSTRACT

Convection, pulsation and magnetic fields have all been suggested as mechanisms for the transport of mass and energy from the optical photosphere of red supergiants, out to the region where the stellar wind is launched. We imaged the red supergiant Betelgeuse at 0.06–0.18 arcsec resolution, using e-Multi-Element Radio-Linked Interferometer Network (e-MERLIN) at 5.5–6.0 GHz, with a sensitivity of $\sim$10 μJy beam$^{-1}$. Most of the radio emission comes from within an ellipse (0.235 × 0.218) arcsec$^2$ ($\sim$5 times the optical radius), with a flux density of 1.62 mJy, giving an average brightness temperature $\sim$1250 K. This radio photosphere contains two hotspots of 0.53 and 0.79 mJy beam$^{-1}$, separated by 90 mas, with brightness temperatures 5400 ± 600 K and 3800 ± 500 K. Similar hotspots, at more than double the distance from the photosphere of those seen in any other regime, were detected by the less-sensitive 'old' MER-LIN in 1992, 1995 and 1996 and many exceed the photospheric temperature of 3600 K. Such brightness temperatures are high enough to emanate from pockets of chromospheric plasma. Other possibilities include local shock heating, the convective dredge-up of hot material or exceptionally cool, low-density regions, transparent down to the hottest layer at $\sim$40 mas radius. We also detect an arc 0.2–0.3 arcsec to the SW, brightness temperature $\sim$150 K, in a similar direction to extensions seen on both smaller and larger scales in the infrared and in CO at mm wavelengths. These preliminary results will be followed by further e-MERLIN, Very Large Array and Atacama Large Millimeter/sub-millimeter Array (ALMA) observations to help resolve the problem of mass elevation from 1 to 10 $R_\star$ in red supergiants.

**Key words:** stars: individual: Betelgeuse – mass-loss – supergiants – radio continuum: stars.

## 1 INTRODUCTION

Betelgeuse (α Ori), type M2Iab, is the closest red supergiant (RSG), with an initial mass of 15–20 M$_\odot$ (Dolan, Mathews & Dearborn 2008). The asymmetric S1 and S2 CO outflows have average velocities and radius limits of 9.8 km s$^{-1}$, 4 arcsec and 14.3 km s$^{-1}$, $\sim$17 arcsec, respectively (O'Gorman et al. 2012). The mass-loss rate $\dot{M}$ of Betelgeuse is $\sim$10$^{-6}$ M$_\odot$ yr$^{-1}$, estimated by Le Bertre et al. (2012) from a 0.24 pc H I shell. Its proper motion is towards the NE and a bow shock was identified in the infrared (IR) (Noriega-Crespo et al. 1997) and H I and mapped using *Herschel* (Decin et al. 2012), which shows arcs 6–7 arcmin NE of the star. We adopt the 2.2 μm photospheric radius $\sim$22.5 milliarcsec (mas)

(Dyck, van Belle & Ridgway 1996; Perrin et al. 2004) as $R_\star$, at a distance of $\sim$197 pc (Harper, Brown & Guinan 2008).

Mass-loss from cool, evolved stars (e.g. VX Sgr) which form copious dust at $\sim$5–10 $R_\star$, is thought to be initiated by pulsations, followed by radiation pressure on dust accelerating the wind to escape velocity (Bowen 1988). However, the requirements for this mechanism do not seem to be present in early M-type stars like Betelgeuse. It shows weaker optical variability (Percy et al. 1996) than the RSG which form more dust. Verhoelst et al. (2006) found signs of metal oxide nucleation at $\sim$1.5 $R_\star$ but silicates have only been found at radii $\gtrsim$500 mas (e.g. Skinner et al. 1997; Tatebe et al. 2007). Dupree et al. (1987) measured periodicities in optical and ultraviolet fluxes probably tracing pulsational shock waves which could help to initiate mass outflow. Other potential mass-loss mechanisms include localized events related to convection (e.g. as modelled by Chiavassa et al. 2010). Aurière et al. (2010)

⋆ E-mail: amsr@jb.man.ac.uk

measured a longitudinal magnetic field of 0.5–1.5 G, leading to models for magnetic promotion of mass-loss (Thirumalai & Heyl 2012). See the Proceedings of the Betelgeuse 2012 workshop, eds. Kervella et al., in preparation, for more comprehensive reviews of mass-loss studies.

Very Large Array (VLA) observations by Lim et al. (1998) at 43, 22, 15, 8 and 5 GHz showed the measured radius increasing from 2 to 7 $R_\star$. The opacity increases with decreasing frequency, so lower frequency images sample layers at larger radii, found to be cooler. Over this range of $R_\star$, the radio brightness temperature $T_b$ falls from ~3540 to 1370 K and the photosphere becomes cool enough for dust to begin to form. However, Uitenbroek, Dupree & Gilliland (1998) detected ultraviolet (UV) continuum and lines formed at $\gtrsim$5000 K, at radii of up to 2.8 and 6 $R_\star$, respectively. Absorption lines reveal a rotation speed of 5 km s$^{-1}$ and they suggest that a bright spot in the SW defines the orientation of the rotational axis, at a position angle (PA) of 55°, giving a deprojected rotation period of 25 yr at 14° yr$^{-1}$. The chromospheric tracer Mg II shows an expansion velocity of 10 km s$^{-1}$, detected out to almost 9 $R_\star$ (Gilliland & Dupree 1996). Asymmetric absorption lines such as H$\alpha$ (Weymann 1962; Bagnulo et al. 2003) suggest outflow of chromospheric material at 5–7 km s$^{-1}$.

Lim et al. (1998) deduced that the chromospheric gas must be at least a thousand times less abundant than the material dominating radio emission, ruling out global heating as a mass-loss mechanism, leaving convection as a plausible alternative. Harper & Brown (2006) studied multi-epoch spatially resolved *Hubble Space Telescope* (*HST*) spectra and, by measuring the electron density and comparing it to 22 GHz observations, confirmed the small filling factor. Chromospheric emission lines suggested rotation about an axis at a PA of 65° at a velocity not exceeding ~5 km s$^{-1}$, suggesting that chromospheric material is not in solid-body rotation at $R > 75$ mas.

We observed Betelgeuse using e-MERLIN at 5.5–6.0 GHz ($\lambda \approx$ 5.2 cm), providing approximately four resolution elements across the stellar diameter. These are the first well-resolved images at cm wavelengths, investigating whether the irregularities seen at 43 GHz ($\lambda$7 mm) persist at larger radii.

## 2  OBSERVATIONS AND DATA REDUCTION

### 2.1  2012 e-MERLIN observations

Betelgeuse was observed in the first semester of e-MERLIN open time on 2012 July 13–15, with a bandwidth of 0.512 GHz centred on 5.75 GHz. Seven antennas were used including the 75 m Lovell telescope providing baselines from 11 to 217 km (90–3910 k$\lambda$). The data were processed in dual polarization, using $4 \times 128$ MHz spectral windows, each divided into 64 2 MHz channels. The point-like QSO 0551+0829, separation 1°.5, was used as the phase reference on a cycle of 7:3 min. OQ208 was used as the bandpass and flux density calibrator. Calibration is summarized in Appendix A. The flux scale is accurate to ~10 per cent and the astrometric uncertainty arising from phase referencing is 16 mas. The calibrated and edited Betelgeuse data comprised 4–8 hr per antenna, spread over 10.5 h, with an average bandwidth of 400 MHz.

We made two maps after self-calibration, using different weighting schemes (see Appendix A). We maximized sensitivity using a 3500 k$\lambda$ taper and a circular 180 mas [full width at half-maximum (FWHM)] restoring beam. This produced a noise $\sigma_{rms}$ 0.027 mJy beam$^{-1}$. We maximized resolution by applying partial uniform weighting (ROBUST 0.75) and using a restoring beam of $(80 \times 60)$ mas$^2$ at PA 143° (close to the natural beam

shape), giving $\sigma_{rms}$ 0.009 mJy beam$^{-1}$. Despite the lower noise per beam, the minimum brightness temperature sensitivity limit is 225 per cent higher with this weighting. In order to ensure artefacts were not introduced, we made images with completely natural weighting (used for astrometry) and with the above weightings, prior to self-calibration. The high-resolution dirty map has $\sigma_{rms}$ of 0.03 mJy beam$^{-1}$, with peaks of 0.81 and 0.63 mJy beam$^{-1}$, similar to the features described in Section 3.3.

### 2.2  Archival data

We retrieved MERLIN Betelgeuse data observed at 4.994 GHz on 1995 June 24 and 1996 Nov 03 (Morris 2001) using 16 MHz bandwidth, and VLA data observed at 4.885 GHz on 1996 Oct 10–21 using 100 MHz bandwidth. These data sets were reduced using standard techniques (Greisen 1994, Diamond et al. 2003). The MERLIN data were imaged with natural weighting [beam size $(85 \times 55)$ mas$^2$] and no cleaning, giving $\sigma_{rms}$ of 0.15 and 0.12 mJy beam$^{-1}$ in 1995 and 1996, respectively. The 1996 MERLIN and VLA data were combined to give a resolution of 200 mas and $\sigma_{rms}$ of 0.058 mJy beam$^{-1}$; the VLA-only image had 400 mas resolution.

## 3  RESULTS

### 3.1  Extended structure seen in 2012

Fig. 1 shows the colour image made with optimum sensitivity to extended structure, using a 180 mas restoring beam. The peak is 1.116 mJy beam$^{-1}$. The $3\sigma_{rms}$ boundary (0.081 mJy beam$^{-1}$ at this resolution), represented by the limit of red shading, has a quite irregular outline, with a maximum extent of 550 mas approximately N–S. The shortest, radial separation between the peak and the $3\sigma_{rms}$ limit is about 190 mas, to the NNE. We fitted a 2D elliptical Gaussian
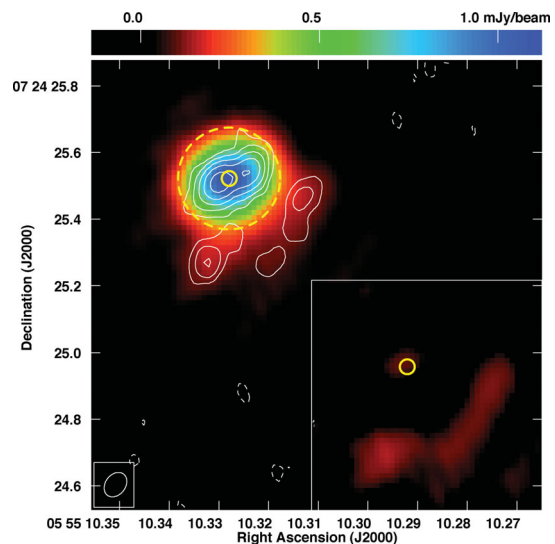


**Figure 1.** The main panel shows the 2012 e-MERLIN colour image of Betelgeuse optimized for sensitivity to extended structure, using a beam size of 180 mas, $\sigma_{rms} = 0.027$ mJy beam$^{-1}$. The contours of the image optimized for resolution are overlaid, with the beam size at lower left, the noise $\sigma_{rms} = 0.009$ mJy beam$^{-1}$ and contour levels at $(-1, 1, 2, 4, 8, 16) \times$ 0.027 mJy beam$^{-1}$. The small, solid yellow circle is the size of the 45 mas diameter photosphere, centred on the low-resolution peak, and the large, dashed circle shows the 310 mas, 5 GHz disc (Lim et al. 1998). The insert shows the SW arc after subtracting the central star, on the same scale.

component to this image, yielding a total flux density $1.619 \pm 0.057$ mJy at position 05:55:10.3274 +07:24:25.514, with a noise-based uncertainty of 4 mas. The component had major and minor axes $(\theta_{\mathrm{maj}}, \theta_{\mathrm{min}})$ of $(235 \times 218)$ mas$^2$, uncertainty $\sigma_\theta = 6$ mas, PA $115 \pm 9°$ (significantly different from the beam PA of $143°$).

The brightness temperature of a component of flux density $S$, area $A$, is given in Kelvin by

$$T_{\mathrm{b}} = 15400 \left( \frac{S}{\mathrm{mJy}} \right) \left( \frac{\lambda}{\mathrm{m}} \right)^2 \left( \frac{A}{\mathrm{arcsec}^2} \right)^{-1} . \qquad (1)$$

We observed at wavelength $\lambda = 0.052$ m. The area of a Gaussian component is given by $A = \pi(\theta_{\mathrm{maj}}\theta_{\mathrm{min}})/(4 \ln 2)$. The main component thus has $T_{\mathrm{b}} = 1170 \pm 135$ K. There is a point-like residual of 0.082 mJy beam$^{-1}$ (only just over $3\sigma_{\mathrm{rms}}$) at the position of the peak, contributing another $\sim$100 K, giving $T_{\mathrm{b}} = 1250 \pm 150$ K within a radius of $\sim$5 $R_\star$. This is close to the temperature and the size (dashed circle in Figs 1–3) measured by Lim et al. (1998) by fitting
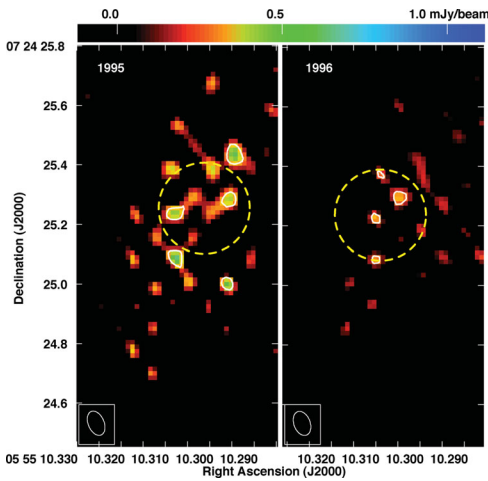


**Figure 2.** MERLIN images of Betelgeuse observed at 4.994 GHz in 1995 and 1996, contours at 0.60 and 0.48 mJy beam$^{-1}$ (4 $\sigma_{\mathrm{rms}}$), respectively, using the same angular scale as Fig. 1. The beam size is $(85 \times 55)$ mas$^2$. The large, dashed circle shows the 310 mas, 5 GHz disc (Lim et al. 1998).
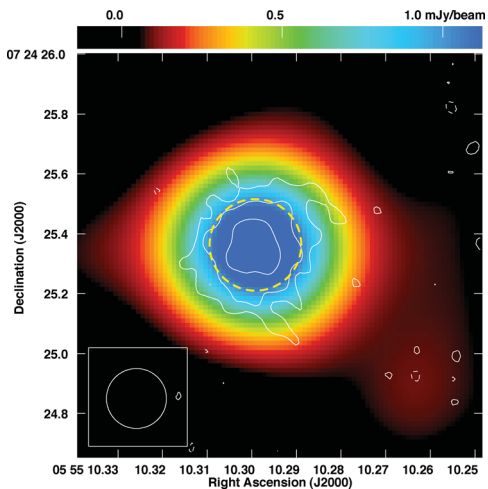


**Figure 3.** 1996 combined MERLIN+VLA image of Betelgeuse [contours at $(-1, 1, 2, 4) \times 0.17$ mJy beam$^{-1}$], beam size 200 mas, overlaid on the VLA-only image observed at 4.9 GHz, beam size 400 mas. The angular scale is the same as Fig. 1. The large, dashed circle shows the 310 mas, 5 GHz disc (Lim et al. 1998).

a uniform disc to the 5 GHz VLA visibilities, showing the stability of these atmospheric conditions over 16 yr.

The residuals after subtracting the central component are shown in the insert of Fig. 1. There is a substantial arc in the SW quadrant, with a maximum extent above $3\sigma_{\mathrm{rms}}$ of 510 mas with a total flux density $0.088 \pm 0.019$ mJy in 0.0249 arcsec$^2$. It has an irregular outline but is approximately 100 mas wide, at a radius between $\sim$175 and 275 mas from the central peak. The SW arc has an average $T_{\mathrm{b}} = 150 \pm 40$ K.

### 3.2 Position and flux density

Our first map of Betelgeuse (phase-reference solutions only) had a peak of $0.78 \pm 0.063$ mJy beam$^{-1}$ at 05:55:10.3267+07:24:25.525. The noise-based position uncertainty is 9 mas and the total astrometric uncertainty (mostly due to the $1°\!.5$ separation from the phase reference source) is 20 mas. Harper et al. (2008) used *Hipparcos* and multi-epoch VLA data to solve for position, proper motion and parallax, up to epoch 2004.829. The preferred solution (their number 5) predicts a position of 05:55:10.3250+07:24:25.536, uncertainty $(5, 6)$ mas at our epoch, 2012.536. This is $(25, 10)$ mas from our position, close to the combined uncertainties.

The total flux density of 1.62–1.71 mJy (depending on whether the SW arc is enclosed) measured at 5.75 GHz, is equivalent to $(1.3–1.4) \pm 0.2$ mJy at 4.85 GHz, using a spectral index of 1.32 (Newell & Hjellming 1982), allowing for the uncertainty in this extrapolation. Observations at 4-8–4.9 GHz showed a decline from 2 to 1.2 mJy during 1981 to 2002, fluctuating within the range 0.9–1.3 mJy up to 2004 (Newell & Hjellming 1982, Skinner et al. 1997, Lim et al. 1998; Harper & Brown private communication).

### 3.3 Hotspots seen in 2012

The contours in Fig. 1 show the image optimized for resolution, using a $(80 \times 60)$ mas$^2$ restoring beam. Two individually unresolved peaks appear, with flux densities and positions of 0.706 mJy beam$^{-1}$ at 05:55:10.3299+07:24:25.510 and 0.489 mJy beam$^{-1}$ at 05:55:10.3241+07:24:25.541, respectively (measured by fitting two Gaussian components simultaneously). $\sigma_{\mathrm{rms}} = 0.0095$ mJy beam$^{-1}$ and the noise-based position uncertainties are 1 mas for the brighter peak and 2 mas for the fainter one. The hotspots are separated by $90 \pm 10$ mas, at a PA of $(110 \pm 10)°$. This is similar to the orientation of the major axis of the Gaussian component fitted to the emission imaged at 180 mas resolution (Section 3.1) and significantly different from the beam PA. The peaks are separated by $>20\sigma$ in both position and flux density. Their brightness temperatures are $T_{\mathrm{b}} = 5400 \pm 600$ K and $T_{\mathrm{b}} = 3800 \pm 500$ K, uncertainties dominated by the overall flux scale uncertainty.

### 3.4 1995–1996 MERLIN and VLA results

Fig. 2 shows that, at the lower sensitivity of the 'old' MERLIN archive data, just a few hotspots were detected at the position of Betelgeuse. In 1995, five spots brighter than 0.60 mJy beam$^{-1}$ ($4\sigma_{\mathrm{rms}}$) were detected, the brightest at 0.78 mJy beam$^{-1}$. In 1996, four spots brighter than 0.48 mJy beam$^{-1}$ ($4\sigma_{\mathrm{rms}}$) were detected, the brightest at 0.56 mJy beam$^{-1}$. The formal position uncertainties are $\sim$40 mas but may be higher due to calibration errors. The shortest baseline (11 km) allows scales as large as 0.5 arcsec to be imaged, and the sensitivity of the 1995 and 1996 images corresponds approximately to the highest contour in Fig. 1, so the non-detection of most of the stellar disc was due to the lack of sensitivity rather than missing spacings. The peak brightness temperatures

(at $\lambda = 0.061$ m) were $T_b = 8000 \pm 2000$ K in 1995 and $T_b = 6000 \pm 2000$ K in 1996. The uncertainties are too high to draw any firm conclusions from the distribution of the spots.

The contours in Fig. 3 show the 1996 combined MERLIN+VLA image, containing $1.69 \pm 0.17$ mJy in a Gaussian component with $(\theta_{maj}, \theta_{min})$ of $(289 \times 256)$ mas$^2$, $\sigma_\theta$ 17 mas, PA $(150 \pm 30)°$. This gives $T_b = 1200 \pm 200$ K. The colour image shows the 1996 VLA-only data, which were part of a multi-frequency data set analysed by Lim et al. (1998) and Harper & Brown (2003), who measured a flux density of $1.77 \pm 0.09$ mJy. The VLA image contains a faint feature 0.6 arcsec due SW of the peak (over twice the distance to the e-MERLIN arc), at 0.095 mJy beam$^{-1}$, just over $3\sigma_{rms}$.

## 4 DISCUSSION

### 4.1 SW Arc

The SW arc is at a radius of $\sim250$ mas, where, according to the semi-empirical model of Harper, Brown & Lim (2001), the electron temperature $T_e$ is $\sim900$ K and the hydrogen number density $n_H \sim 5 \times 10^{13}$ m$^{-3}$. This gives an optical depth $\sim0.18$ for the observed $T_b \sim 150$ K. Assuming that the arc is as deep as it is wide, we approximate the region producing most of the emission by a spheroid with semimajor axes of 10, 10 and 25 au, giving a hydrogen mass of $\sim1.8 \times 10^{-6}$ M$_\odot$, suggesting that one such clump could be formed every couple of years.

The arc is about 100 mas outside the 6 GHz photospheric radius, in a similar direction to the CN plume seen by Kervella et al. (2009) at $\lesssim 6$ $R_\star$ and the faint SW extension at $\sim0.6$ arcsec seen at 5 GHz in 1996. A clump of CO emission was seen in 2007 by O'Gorman et al. (2012) just outside the S1 shell, 5 arcsec SW of the centre, suggesting a wind travel time of $\sim500$ yr at 9 km s$^{-1}$. These observations suggest repeated or continuous ejections, rather than proper motion of a single clump. This is also aligned with the SW pole of the rotational axis identified by Uitenbroek et al. (1998). The direction could be coincidence, since observations at 7.76–19.5 μm in 2010 Nov (Kervella et al. 2011) show clumps outside the photosphere at 0.8–1.7 arcsec around more than a semicircle, between NE and S. A comparison with the direction of the bow shock seen 6–7 arcmin to the NE (Decin et al. 2012) is tempting, but structures on sub-arcmin scales are deep within the astropause and should share the proper motion of the star.

### 4.2 Hotspots

The 5–6 GHz hotspots, measured at 55–85 mas resolution, have $T_b$ formally above the peak photospheric temperature of 3600 K (Dyck et al. 1996), similar to the chromospheric temperature, which could reach 8000 K (Harper & Brown 2006). We used conservative uncertainties, dominated by the maximum uncertainty in the flux scale, although the good agreement with VLA results for the whole-disc flux density suggests that our uncertainties may be overestimated. One or more hotspots are significantly hotter than the photosphere in 2012, 1996 and 1995 and also in the 1992 MERLIN observations imaged at full resolution (Morris 2001). Note that, at the sensitivity of old MERLIN, no emission at all at $T_b \lesssim 4500$–6000 K (depending on epoch) would have been detected.

The radio photosphere major axis is at 110–115° in the fully calibrated 2012 data, compared with $(67 \pm 7)°$ at 43 GHz in 1998 (Lim et al. 1998). The orientation of the optical disc and hot spots also varies; the $\sim20$ mas axis joining the two hotspots seen by Haubois et al. (2009) is approximately NE–SW. Four sets of IR

observations over 24 months by Tuthill, Haniff & Baldwin (1997) showed 2–3 hotspots at a variety of PAs within the inner $\sim100$ mas.

Harper & Linsky (2001) showed that increasing the local $T_e$ 2–3 fold enhances radio emission much more effectively than increasing the gas density by the same factor. There are several possible origins for hotspots.

(i) Levitation of gas from the inner photosphere, e.g. by convection, although such gas would cool radiatively and by expansion.

(ii) Exceptionally cool, small patches in the outer layers, transparent enough to expose hotter, inner layers. The separation of the 2012 hotspots is $90 \pm 10$ mas, similar to the 80 mas diameter of the hottest layer (where the greatest chromospheric contribution to emission is greatest, Harper & Brown 2006, using 197 pc distance).

(iii) Shock heating due to pulsations and/or convection.

(iv) Chromospheric patches at $\sim5$ $R_\star$ heated by acoustic and/or magnetic processes.

Options (iii) and/or (iv) seem most likely to produce radio hotspots $\gtrsim4000$ K. Ireland, Scholz & Wood (2011) modelled pulsation in Miras out to $5R_\star$, finding average effective temperatures $\leq3800$ K. Large-scale up- and down-flows are seen in chromospheric lines, including directional reversals at up to $\sim3R_\star$, measured by Lobel & Dupree (2001). Ohnaka et al. (2011) measured up- and down-draughts of CO, within $\sim2.5R_\star$, at $\lesssim30$ km s$^{-1}$, with different velocities occurring simultaneously on different sides of the star. Such speeds are sufficient to supply shock heating even if it is not clear how convection could operate at $\gg2.5R_\star$. Wittkowski et al. (2011) made spectro-interferometric observations, around 2 μm, of continuum and clumpy molecular layers around AGB stars, which suggested pulsation- and shock-induced chaotic motion, not requiring convection. The bulk of the radio emission is non-chromospheric (Section 1), but the hotspots have $T_b \lesssim 8000$ K, in the chromospheric range. Harper & Brown (2006) suggest that chromospheric gas is confined within magnetic fields; dissipation of magnetic energy may continue to heat the gas even at high elevations.

## 5 FURTHER HIGH-RESOLUTION STUDIES

We have shown that both cool, extended radio-continuum emission and hot starspots on Betelgeuse can be resolved at 5.5–6 GHz. Multi-epoch, multifrequency follow-up is needed to establish the emission mechanisms and role in mass-loss. In full operations, e-MERLIN will reach 0.002 mJy beam$^{-1}$ in two full tracks at 5–7 GHz. Proper motions of 5 km s$^{-1}$ could be measured in four months for a spot 0.3 mJy brighter than its surroundings, revealing whether the hotspots rotate as predicted for the chromosphere. The variability time-scale will constrain the underlying mechanism. Modelling by Harper & Linsky (2001) shows that C II recombination to C I takes $\sim2$ months at $n_H \sim 4 \times 10^{14}$ m$^{-3}$, around 5 $R_\star$, or longer at higher radius, and chemical changes have similar time-scales, but mechanisms involving bulk up-/down-draughts alone would take about a year to produce comparable changes.

Matching resolution at 50 mas can be achieved by the EVN, e-MERLIN and the Karl G. Jansky VLA (alone or in combination as required) at 1.4–50 GHz, and eventually by Atacama Large Millimeter/sub-millimeter Array (ALMA) at higher frequencies. Finer resolution ($\leq20$ mas) is possible at 22 GHz and some higher frequencies, suited to the smaller observed size of the radio photosphere. This will allow us to resolve the spectral indices of the extended emission and the hotspots and test models for localized heating (Harper et al. 2001) and references therein). For example,

a decrease of $T_e$ with decreasing frequency above a hotspot would suggest a chromospheric, rather than convective origin.

The average radius (Lim et al. 1998) is approximately related to the observing frequency in GHz by $R(\nu) \sim 55\nu^{-0.5}$ au. At a speed of $10\,\mathrm{km\,s^{-1}}$ (within the range shown by chromospheric lines, Gilliland & Dupree 1996), it would take 0.5 yr for a disturbance to propagate 1 au from surfaces optically thick at 25 GHz to 21 GHz, and 1 yr from the 6 GHz to the 5 GHz surface. Monitoring at decreasing frequencies, i.e. increasing radii, at suitable intervals, will track the evolution of disturbances. This will show whether we are witnessing phenomena propagating outwards smoothly, or localized changes behaving differently, helping to distinguish between convection and pulsation. We will resolve CO, other molecules and dust using ALMA, thus measuring the composition and mass of the wind. Clumps will be resolved on scales of a few au, within a few tens au from the star, where chemistry is still active, overlapping with the scales resolved in the mid-IR (Kervella et al. 2011).

## 6 SUMMARY

e-MERLIN has produced the highest resolution images of Betelgeuse at cm wavelengths, in 2012 July. The 5.75 GHz photosphere is fitted by a 2D Gaussian component, axes $(0.235 \times 0.218)$ arcsec$^2$ $(\sim 5R_\star)$, flux density 1.62 mJy, with an average brightness temperature $\sim 1250$ K. Extrapolating to 4.9 GHz shows that the flux density decline since 1981 may have levelled off; the large-scale size and brightness is consistent with the results from Lim et al. (1998). The peak position is close to the position predicted from the proper motion analysis by Harper et al. (2008). An arc is seen 0.2–0.3 arcsec to the SW, brightness temperature $\sim 150$ K, hydrogen mass $\sim 1.8 \times 10^{-6}$ M$_\odot$. It is in the same direction as IR plumes seen on smaller and larger scales (Kervella et al. 2009, 2011;), a faint 4.9-GHz feature at 0.6 arcsec seen in 1996 and CO emission imaged by O'Gorman et al. (2012). This suggests persistent ejection in this direction for several centuries.

e-MERLIN resolved two distinct peaks, 90 mas apart within the larger stellar disc, with brightness temperatures 4000–6000 K. These are likely to be hotspots at $\sim 5\,R_\star$, although it is possible that cooler, low-opacity inhomogeneities in higher layers reveal the hottest chromospheric layers. Similar, isolated peaks were also detected by MERLIN observations in 1992, 1995 and 1996. Such high-sensitivity, high-resolution radio continuum observations can resolve emission simultaneously from material at chromospheric and photospheric temperatures, and have the potential to track proper motions. Future multifrequency imaging with e-MERLIN, the VLA and ALMA will investigate whether the signatures of chromospheric emission, convection or pulsation shocks are seen in the radio photosphere from 2–10 $R_\star$, helping to elucidate the mechanisms which eject material from the star into its envelope.

## REFERENCES

Aurière M., Donati J.-F., Konstantinova-Antova R., Perrin G., Petit P., Roudier T., 2010, A&A, 516, L2

Bagnulo S. et al., 2003, Messenger, 114, 10
Bowen G. H., 1988, ApJ, 329, 299
Chiavassa A. et al., 2010, A&A, 511, A51
Decin L. et al., 2012, A&A, 548, 113
Diamond P. J. et al., 2003, MERLIN User Guide, JBO, Macclesfield
Dolan M., Mathews G. J., Dearborn D., 2008, Nuclei in the Cosmos, Proc. Sci., 53, 242
Dupree A. K., Baliunas S. L., Hartmann L., Nassiopoulos G. E., Guinan E. F., Sonneborn G., 1987, ApJ, 317, L85
Dyck H. M., van Belle G. T., Ridgway S. T., 1996, AJ, 111, 1705
Gilliland R. L., Dupree A. K., 1996, ApJ, 463, L29
Greisen E., ed. 1994, AIPS Cookbook. NRAO, Charlottesville
Harper G. M., Brown A., 2003, in Piskunov N., Weiss W. W., Gray D. F., eds, Modelling of Stellar Atmospheres. Astron. Soc. Pac., San Francisco, p. 11
Harper G. M., Brown A., 2006, ApJ, 646, 1179
Harper G. M., Linsky J. L., 2001, in Garcia Lopez R. J., Rebolo R., Zapaterio Osorio M. R., eds, 11th Cambridge Workshop on Cool Stars, Stellar Systems and the Sun. Vol. 223. Astron. Soc. Pac., San Francisco, p. 1603
Harper G. M., Brown A., Lim J., 2001, ApJ, 551, 1073
Harper G. M., Brown A., Guinan E. F., 2008, AJ, 135, 1430
Haubois X. et al., 2009, A&A, 508, 923
Ireland M. J., Scholz M., Wood P. R., 2011, MNRAS, 418, 114
Kervella P., Verhoelst T., Ridgway S. T., Perrin G., Lacour S., Cami J., Haubois X., 2009, A&A, 504, 115
Kervella P., Perrin G., Chiavassa A., Ridgway S. T., Cami J., Haubois X., Verhoelst T., 2011, A&A, 531, A117
Le Bertre T., Matthews L. D., Gérard E., Libert Y., 2012, MNRAS, 422, 3433
Lim J., Carilli C. L., White S. M., Beasley A. J., Marson R. G., 1998, Nat., 392, 575
Lobel A., Dupree A. K., 2001, ApJ, 558, 815
Morris R. a. H., 2001, PhD thesis, University of Wales, Cardiff
Newell R. T., Hjellming R. M., 1982, ApJ, 263, L85
Noriega-Crespo A., van Buren D., Cao Y., Dgani R., 1997, AJ, 114, 837
O'Gorman E., Harper G. M., Brown J. M., Brown A., Redfield S., Richter M. J., Requena-Torres M. A., 2012, AJ, 144, 36
Ohnaka K. et al., 2011, A&A, 529, A163
Percy J. R., Desjardins A., Yu L., Landis H. J., 1996, PASP, 108, 139
Perrin G., Ridgway S. T., Coudé du Foresto V., Mennesson B., Traub W. A., Lacasse M. G., 2004, A&A, 418, 675
Skinner C. J., Dougherty S. M., Meixner M., Bode M. F., Davis R. J., Drake S. A., Arens J. F., Jernigan J. G., 1997, MNRAS, 288, 295
Tatebe K., Chandler A. A., Wishnow E. H., Hale D. D. S., Townes C. H., 2007, ApJ, 670, L21
Thirumalai A., Heyl J. S., 2012, MNRAS, 422, 1272
Tuthill P. G., Haniff C. A., Baldwin J. E., 1997, MNRAS, 285, 529
Uitenbroek H., Dupree A. K., Gilliland R. L., 1998, AJ, 116, 2501
Verhoelst T. et al., 2006, A&A, 447, 311
Weymann R., 1962, ApJ, 136, 844
Wittkowski M. et al., 2011, A&A, 532, L7